American Mineralogist, Volume 107, pages 1952–1959, 2022

Zinconigerite-2*N*1*S* $ZnSn_2Al_{12}O_{22}(OH)_2$ and zinconigerite-6*N*6*S* $Zn_3Sn_2Al_{16}O_{30}(OH)_2$, two new minerals of the nolanite-spinel polysomatic series from the Xianghualing skarn, Hunan Province, China

Can Rao[1,*], Xiangping Gu[2], Rucheng Wang[3], Qunke Xia[1,†], Chuanwan Dong[1], Frédéric Hatert[4], Fabrice Dal Bo[5], Xuege Yu[1], and Wumengyu Wang[1]

[1]Key Laboratory of Geoscience Big Data and Deep Resource of Zhejiang Province, School of Earth Sciences, Zhejiang University, Hangzhou 310027, China
[2]School of Earth Sciences and Info-physics, Central South University, Changsha, 410083, China
[3]State Key Laboratory for Mineral Deposits Research, School of Earth Sciences and Engineering, Nanjing University, Nanjing, 210046, China
[4]Laboratoire de Minéralogie, B18, Université de Liège, B-4000 Liège, Belgium
[5]Natural History Museum, University of Oslo, PO 1172 Blindern, 0318 Oslo, Norway

Abstract

Zinconigerite-2*N*1*S* $ZnSn_2Al_{12}O_{22}(OH)_2$ and zinconigerite-6*N*6*S* $Zn_3Sn_2Al_{16}O_{30}(OH)_2$ are two new minerals with different numbers and ratios of nolanite (*N*) and spinel (*S*) modules. Both phases have been discovered in the Xianghualing skarn, Hunan Province, China. Zinconigerite-2*N*1*S* (zn-2*N*1*S*) and zinconigerite-6*N*6*S* (zn-6*N*6*S*) are named for their chemical composition, number, and ratios of *N*-*S* modules, according to the nomenclature of the nolanite-spinel polysomatic series of Armbruster (2002). Both phases occur as aggregates, sub-to-euhedral crystals, with maximal dimensions up to 100 μm, within fluorite aggregates, and they are closely associated with phlogopite, chrysoberyl, magnetite, cassiterite, margarite, and nigerite-taaffeite group minerals. They do not show fluorescence in long- or short-wave ultraviolet light. The calculated densities are 4.456 g/cm^3 for zn-2*N*1*S* and 4.438 g/cm^3 for zn-6*N*6*S*. Optically, zn-2*N*1*S* is uniaxial (+) with ω = 1.83(1), ε = 1.84(2); zn-6*N*6*S* is uniaxial (+) with ω = 1.85(1), ε = 1.87(2) (λ = 589 nm). Their chemical compositions by electron-microprobe analyses give the empirical formulas $(Zn_{0.734}Mn_{0.204}Na_{0.122}Ca_{0.063}Mg_{0.044})_{\Sigma 1.166}(Sn_{1.941}Zn_{0.053}Ti_{0.007})_{\Sigma 2}(Al_{11.018}Fe^{3+}_{0.690}Zn_{0.200}Si_{0.092})_{12}O_{22}(OH)_2$ for zn-2*N*1*S* and $(Zn_{1.689}Mn_{0.576}Mg_{0.328}Fe^{3+}_{0.407})_{\Sigma 3}(Sn_{1.882}Zn_{0.047}Ti_{0.071})_{\Sigma 2}(Al_{14.675}Fe^{3+}_{1.088}Na_{0.13}Ca_{0.086}Si_{0.017})_{\Sigma 15.996}O_{30}(OH)_2$ for zn-6*N*6*S*. Both phases have trigonal symmetry; the unit-cell parameters of zn-2*N*1*S* ($P\bar{3}m1$) and zn-6*N*6*S* ($R\bar{3}m$), refined from single-crystal X-ray diffraction data, are, a = 5.7191(2) and 5.7241(2) Å, c = 13.8380(6) and 55.5393(16) Å, V = 391.98(3) and 1575.96(12) Å^3, and Z = 1 and 3, respectively. The structure of zn-2*N*1*S* is characterized by the alternating O-T_1-O-T_2-O-T_1 layers stacked along the *c*-axis, showing the connectivity of *N*-*S*-*N*. The polyhedral stacking sequence of zn-6*N*6*S* is 3 × (O-T_1-O-T_2-O-T_2-O-T_1), reflecting a *N*-*S*-*S*-*N*-*N*-*S*-*S*-*N*-*N*-*S*-*S*-*N* connectivity of the polysomatic structure. By contrast, the structure of zn-2*N*1*S* shows the elemental replacements of Al → Sn and Al → Zn, suggesting the substitution mechanism of 2Al → Zn + Sn. The complex substitution of Zn by multiple elements (Al, Fe^{3+}, Mn, Mg) in the structure of zn-6*N*6*S*, is coupled with the low occupancy of Al5-octahedra. Fe^{3+} → Al substitution occurs in Al1-tetrahedra of both zn-2*N*1*S* and zn-6*N*6*S*. The new polysomes, zn-2*N*1*S* and zn-6*N*6*S*, likely crystallized under F-rich conditions during the late stages of the Xianghualing skarn formation. The discovery of zn-2*N*1*S* and zn-6*N*6*S* provides new insights into the crystal chemistry of the *N*-*S* polysomatic series and its origin.

Keywords: Zinconigerite-2*N*1*S*, zinconigerite-6*N*6*S*, nolanite module, spinel module, polysomatic series, Xianghualing skarn

Introduction

Minerals of the nigerite and högbomite groups are included in a polysomatic series that comprises nolanite and spinel structural blocks. The structures of nigerite and högbomite group minerals are constructed by the regular stacking of (001) slabs of a nolanite module and (111) slabs of a spinel module (Armbruster 2002). The nolanite module consists of a layer of octahedrally coordinated cations (O-layer) and a layer of both tetrahedrally and octahedrally coordinated cations with an OH group (T_1-layer), whereas the spinel module consists of an O-layer and a layer of both tetrahedrally and octahedrally coordinated cations (T_2-layer) (Fig. 1). If Sn > Ti in the nolanite module, these minerals belong to the nigerite group; however, if Ti > Sn in the nolanite module, they belong to the högbomite group. Different chemical compositions, numbers and ratios of nolanite and spinel blocks differentiate members of the nigerite and högbomite groups, such as magnesionigerite-2*N*1*S* (Chen et al. 1989), magnesionigerite-6*N*6*S* (Yang et al. 2013),

* E-mail: canrao@zju.edu.cn
† Orcid 0000-0003-1256-7568

0003-004X/22/0010–1952$05.00/DOI: https://doi.org/10.2138/am-2022-7983

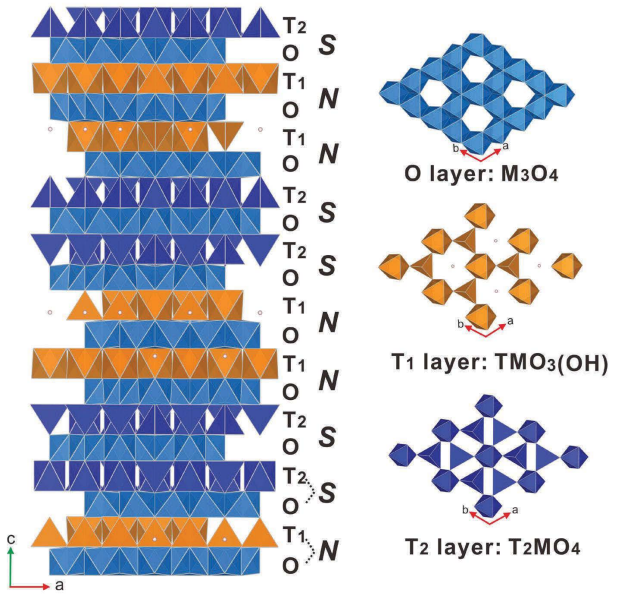

Figure 1. Schematic representation of the structure ([001] projection) of nigerite-högbomite group minerals in terms of nolanite(*N*)-spinel(*S*) modules. (Color online.)

ferronigerite-2*N*1*S* (Bannister et al. 1947; Jacobson and Webb 1947), ferronigerite-6*N*6*S* (Peacor 1967; Burke et al. 1977), magnesiohögbomite-2*N*2*S* (McKie 1963), magnesiohögbomite-2*N*3*S* (Hejny and Armbruster 2002), magnesiohögbomite-6*N*6*S* (Schmetzer and Berger 1990), zincohögbomite-2*N*2*S* (Ockenga et al. 1998), and zincohögbomite-2*N*6*S* (Armbruster et al. 1998). The polysomes of zn-2*N*1*S* and zn-6*N*6*S* have been predicted as members of the nigerite group by Armbruster (2002), but they were not previously discovered.

The recent discovery of two new *N*-*S* type minerals from the Xianghualing skarn (Linwu County, Hunan Province, southern China), zn-2*N*1*S* and zn-6*N*6*S*, led to the definition of two new species, which were approved by the Commission on New Minerals, Nomenclature and Classification, IMA (2018-037 and 2018-122a, respectively) (Rao et al. 2018, 2020b). The holotype material has been deposited in the collections of the Geological Museum of China, No. 15 Building, Yangrou Hutong Road, Xisi, Beijing 100031, People's Republic of China, under catalog number M13810 (zn-2*N*1*S*) and M13811 (zn-6*N*6*S*). The chemical composition and crystal structure were determined using electron probe microanalysis (EPMA) and single-crystal X-ray diffraction (SC-XRD), respectively. This paper describes the chemical and structural information of zn-2*N*1*S* and zn-6*N*6*S*, and discusses the composition, crystal chemistry and crystal structure of *N*-*S* polysomatic series and their petrological origin.

Geological setting, occurrence, and paragenesis

The Xianghualing skarn is a tin-polymetallic (Sn-W-Be-Li) deposit in Linwu County, Hunan Province, southern China. It occurs in the exocontact zone between the Laiziling granitic pluton and the Middle-Upper Devonian carbonate rocks of the Qiziqiao Formation (Huang et al. 1988). The U-Pb dating of the zircon of the protolithionite granite from the Laiziling granitic pluton indicates the age of 155 Ma (Zhu et al. 2011). The Laiziling granite is enriched in the elements Li, Be, Sn, W, Rb, Nb, and Ta; it is generally regarded as the main Sn source of the Xianghualing orebodies (Huang et al. 1988). The granite has an average Sn concentration of 65 ppm (Zhong 2014). The predominant accessory minerals in the Xianghualing skarn include Sn minerals (cassiterite, hulsite, and nigerite group minerals), W minerals (wolframite and scheelite), Be minerals (hsianghualite, liberite, chrysoberyl, hambergite, bertrandite, and taaffeite group minerals), and Li minerals (hsianghualite and liberite). The Xianghualing skarn is the type locality for five minerals species: hsianghualite $Ca_3Li_2Be_3(SiO_4)_3F_2$ (Huang et al. 1958), liberite $Li_2Be(SiO_4)$ (Chao 1964), ferrotaaffeite-2*N*′2*S* $BeFe_3Al_8O_{16}$ (Yang et al. 2012), mengxianminite $Ca_2Sn_2Mg_3Al_8[(BO_3)(BeO_4)O_6]_2$ (Rao et al. 2017), and chukochenite $LiAl_5O_8$ (Rao et al. 2020a).

Both zn-2*N*1*S* and zn-6*N*6*S* occur as aggregates, sub-to-euhedral crystals, with maximal dimensions up to 100 μm, and are found within fluorite aggregates (Fig. 2). The crystals have a stout prismatic morphology, elongated along [001]. Zn-2*N*1*S* is closely associated with fluorite, phlogopite, chrysoberyl, ferronigerite-2*N*1*S*, magnetite, cassiterite, magnesiotaaffeite-2*N*′2*S*, and margarite (Figs. 2a and 2b). Zn-6*N*6*S* occurs as crystals in interstices of fluorite (Figs. 2c and 2d), or with ferronigerite-2*N*1*S* in veinlets or aggregates in fluorite, in close association with phlogopite, chrysoberyl, ferronigerite-6*N*6*S*, and ferronigerite-2*N*1*S*. Intimate intergrowths with hydrothermal minerals such as fluorite and phlogopite indicate that zn-2*N*1*S* and -6*N*6*S* are of hydrothermal origin in the Xianghualing skarn.

Crystal chemistry

Chemical composition

The chemical compositions of zn-2*N*1*S*, zn-6*N*6*S*, and coexisting minerals were obtained on polished samples. The analyses were performed using a SHIMADZU EPMA 1720H electron microprobe at the EPMA Lab in the School of Earth Sciences, Zhejiang University, operating in wavelength-dispersive mode at 15 kV, 20 nA beam current, 1 μm beam diameter, and 20 and 10 s counting times on peak and background regions, respectively. The analytical standards used were orthoclase (Na*K*α), $MnTiO_3$ (Ti*K*α), almandine (Ca*K*α and Fe*K*α), obsidian (K*K*α), pyrope (Mg*K*α), willemite (Mn*K*α, Zn*K*α, and Si*K*α), topaz (Al*K*α), cassiterite (Sn*K*α), and apatite (F*K*α). F was not detected in either zn-2*N*1*S* or zn-6*N*6*S*. According to the crystal-stoichiometrical features of zn-2*N*1*S* and zn-6*N*6*S* (see below), Fe is required to be Fe^{3+}, thus FeO contents were stoichiometrically converted to Fe_2O_3. The contents of H_2O were calculated based on 2 (OH) groups per formula unit (pfu). The chemical analysis results of zn-2*N*1*S* and zn-6*N*6*S* are summarized in Table 1.

The empirical formula for zn-2*N*1*S* (based on 24 O apfu) is $(Zn_{0.734}Mn_{0.204}Na_{0.122}Ca_{0.063}Mg_{0.044})_{\Sigma 1.166}(Sn_{1.941}Zn_{0.053}Ti_{0.007})_{\Sigma 2}(Al_{11.018}Fe^{3+}_{0.690}Zn_{0.200}Si_{0.092})_{\Sigma 12}O_{22}(OH)_2$. The ideal end-member formula is $ZnSn_2Al_{12}O_{22}(OH)_2$, which requires Al_2O_3 60.30 wt%, SnO_2 29.71 wt%, ZnO 8.02 wt%, and H_2O 1.97 wt%. The empirical formula calculated from the chemical analyses of

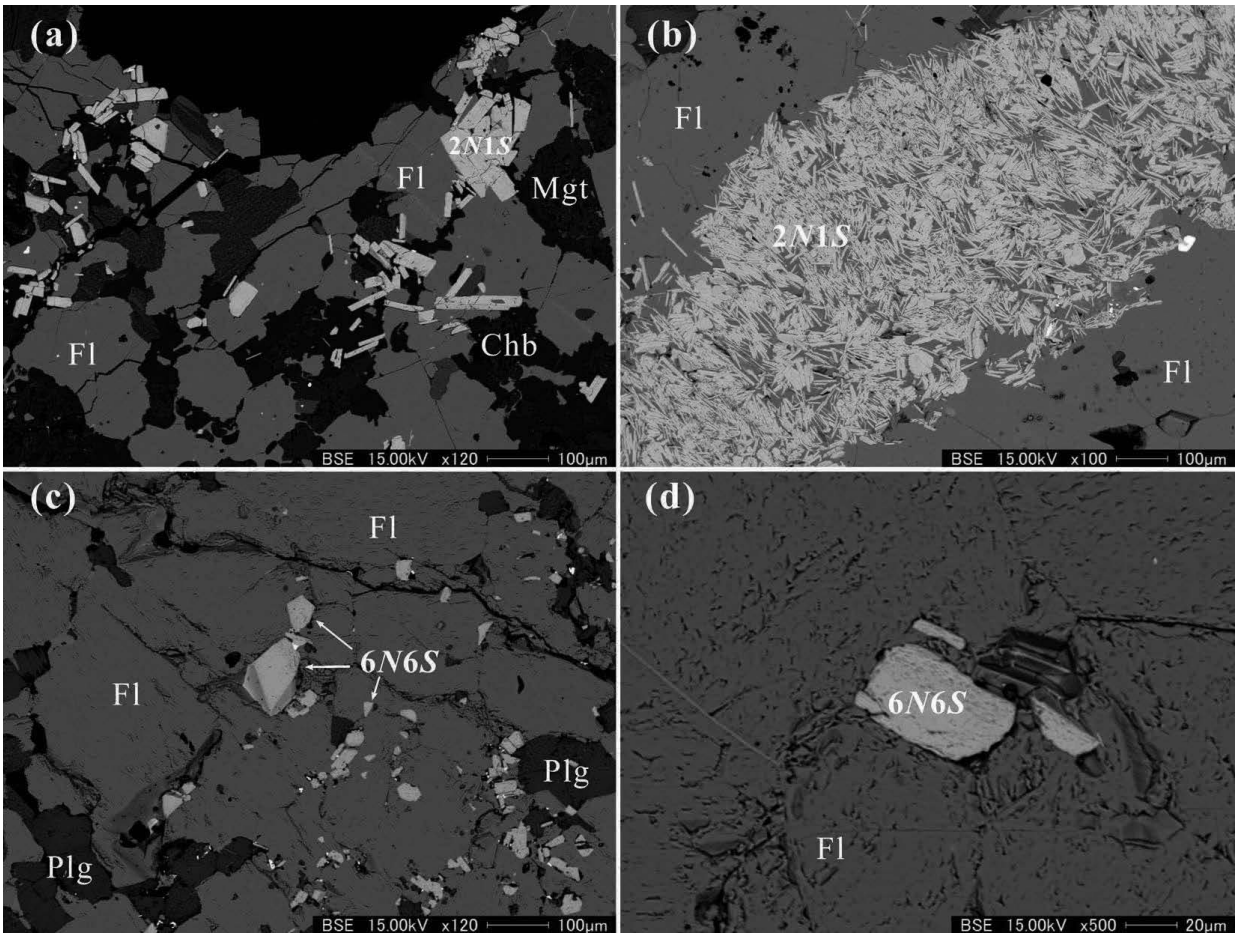

Figure 2. Backscattered electron (BSE) images showing occurrence and mineral associations of zinconigerite-2*N*1*S* and -6*N*6*S* from the Xianghualing skarn. (**a**) Euhedral zinconigerite-2*N*1*S* crystals among fluorite crystals; (**b**) Zinconigerite-2*N*1*S* crystal veinlets among fluorite; (**c** and **d**) euhedral zinconigerite-6*N*6*S* crystals among fluorite crystals. Abbreviations: 2*N*1*S* = zinconigerite-2*N*1*S*; 6*N*6*S* = zinconigerite-6*N*6*S*; Fl = fluorite; Mgt = margarite; Chb = chrysoberyl; Plg = phlogopite.

zn-6*N*6*S* (based on 32 O apfu) is $(Zn_{1.689}Mn_{0.576}Mg_{0.328}Fe^{3+}_{0.407})_{\Sigma 3}(Sn_{1.882}Zn_{0.047}Ti_{0.071})_{\Sigma 2}(Al_{14.675}Fe^{3+}_{1.088}Na_{0.13}Ca_{0.086}Si_{0.017})_{\Sigma 15.996}O_{30}(OH)_2$. The ideal end-member formula is $Zn_3Sn_2Al_{16}O_{30}(OH)_2$, which requires Al_2O_3 59.05 wt%, SnO_2 21.82 wt%, ZnO 17.68 wt%, and H_2O 1.45 wt%.

Physical and optical properties

The crystals of both zn-2*N*1*S* and zn-6*N*6*S* are green and translucent-to-transparent, with a vitreous luster. The tenacities are brittle, and the fractures are irregular. Neither crystal shows fluorescence in long- or short-wave ultraviolet light. Based on the empirical formula and single-crystal unit-cell parameters, the calculated densities are 4.456 g/cm^3 for zn-2*N*1*S* and 4.438 g/cm^3 for zn-6*N*6*S*. Optically, zn-2*N*1*S* is uniaxial positive, with ω = 1.83 (1), ε = 1.84 (2); zn-6*N*6*S* is also uniaxial positive, with ω = 1.85 (1), ε = 1.87 (2) under sodium light (λ = 589 nm). The optical orientation is α//*a*, β//*b*, and γ//*c*. According to the calculated density and the measured indexes of refraction, the compatibility indices $[1 - (K_P/K_C)]$ of zn-2*N*1*S* and zn-6*N*6*S* are 0.024 and 0.028, respectively, corresponding to the "excellent" category (Mandarino 1981).

Raman spectroscopy

Raman spectra of zn-2*N*1*S* and zn-6*N*6*S* were collected using a LabRAM HR evolution Laser Raman microprobe in the School of Earth Sciences at Zhejiang University. A 532 nm laser with a power of 50 mW at the sample surface was used. Silicon (520 cm^{-1} Raman shift) was used as a standard. Raman spectra were acquired on polished thin sections from 100 to 4000 cm^{-1}, and the accumulation time of each spectrum was 60 s (Fig. 3). The presence of (OH) groups is confirmed by the Raman shifts at 3476, 3617, and 3699 cm^{-1} for zn-2*N*1*S* (Fig. 3a) and at 3478 cm^{-1} for zn-6*N*6*S* (Fig. 3b). The bands in the region 700–850 cm^{-1} are assigned to the stretching modes v_1 and v_3 of (AlO_6) groups, and the bending modes v_2 and v_4 of (AlO_6) groups in the region of 500–300 cm^{-1}. The Zn-O vibration modes are probably at the bands of 634–614 cm^{-1}. The lattice vibration modes occur below 310 cm^{-1}.

X-ray crystallography and structure determination

Both powder and single-crystal X-ray diffraction studies were carried out on zn-2*N*1*S* and zn-6*N*6*S*. Powder X-ray diffraction patterns were collected using a Rigaku D/max Rapid

TABLE 1. Chemical data of zinconigerite-2*N*1*S* and zinconigerite-6*N*6*S* from the Xianghualing skarn

Constituent wt%	Zinconigerite-2*N*1*S* n = 20	Zinconigerite-6*N*6*S* n = 47
Al_2O_3	54.42(0.01)	54.12(0.62)
SnO_2	28.15(0.56)	20.54(0.51)
ZnO	7.71(0.22)	10.22(0.33)
Fe_2O_3[a]	5.83(0.38)	8.65(0.51)
MnO	1.39(0.42)	2.95(0.49)
MgO	0.17(0.04)	0.96(0.13)
TiO_2	0.05(0.05)	0.41(0.19)
SiO_2	0.53(0.26)	0.07(0.06)
CaO	0.34(0.07)	0.35(0.47)
K_2O	0.00(0.00)	0.00(0.01)
Na_2O	0.36(0.14)	0.36(0.13)
H_2O[b]	1.73(0.01)	1.45(0.01)
Total	100.68(0.46)	100.09(0.61)
	O = 24	O = 32
Al (apfu)	11.174	14.675
Sn	1.952	1.882
Zn	0.992	1.736
Fe^{3+}	0.771	1.495
Mn	0.206	0.576
Mg	0.044	0.328
Ti	0.007	0.071
Si	0.092	0.017
Ca	0.063	0.086
K	0.000	0.001
Na	0.123	0.160
H	2.000	2.000

Notes: n = number of analyses; values in parentheses = standard deviation.
[a] Calculated as Fe^{3+}.
[b] H_2O calculated on the basis of 2 (OH) apfu.

IIR micro-diffractometer (Cu*K*a, λ = 1.54056 Å) for zn-2*N*1*S* and a Rigaku D/MAX Rapid II micro-diffractometer (Mo*K*α, λ = 0.71073 Å) for zn-6*N*6*S*. Single-crystal X-ray diffraction data for both zn-2*N*1*S* and zn-6*N*6*S* were collected on a Rigaku Synergy diffractometer (Mo*K*α, 50 kV, 1 mA) in the School of Earth Sciences and Info-physics, Central South University (China). The Rigaku CrystalClear software package was used to process structural data, as well as applying Lorentz and polarization corrections. An empirical absorption correction was applied using the ABSCOR (Higashi 2001) software multi-scan method. Scattering curves for neutral atoms, together with anomalous dispersion corrections, were taken from the *International Tables for X-ray Crystallography (Volume C)* (Wilson 1992). Online Materials[1] CIF is available.

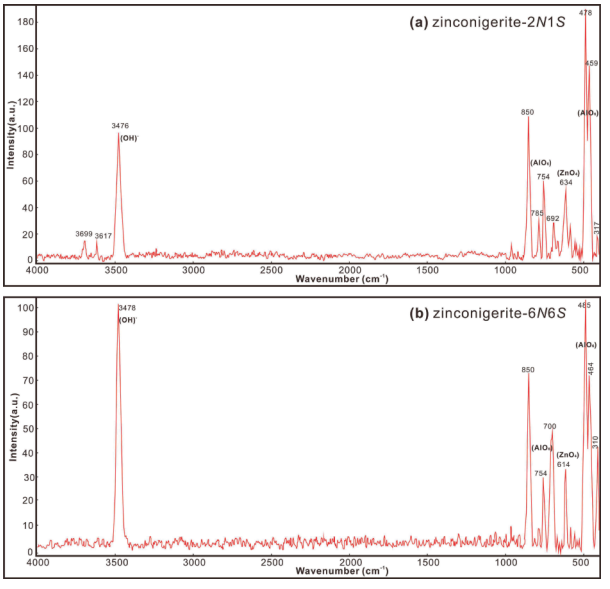

FIGURE 3. Raman spectra of zinconigerite-2*N*1*S* (**a**) and zinconigerite-6*N*6*S* (**b**) from the Xianghualing skarn. (Color online.)

Zinconigerite-2*N*1*S*. Single-crystal X-ray diffraction was obtained on a zn-2*N*1*S* crystal fragment measuring 0.120 × 0.075 × 0.050 mm. A total of 3010 reflections were extracted from 624 frames, corresponding to 570 unique reflections. The unit-cell parameters, calculated by least-squares refinement from these reflections, are a = 5.7191(2) Å, c = 13.8380(6) Å, V = 391.98(3) Å^3, and Z = 1. The structure, which has a trigonal symmetry, was refined in the space group $P\bar{3}m1$. During the final refinement cycles, all the atoms were refined anisotropically. R_1 [F_o >2s(F_o)] value of 0.0296 and wR_2 value of 0.0967 were obtained. Site occupancies were established by comparing chemical data, site scattering factors, and average bond distances (Table 2a). Selected

TABLE 2a. Assigned site-occupancies in the crystal structure of zinconigerite-2*N*1*S*

Site	RSS	Site population (apfu)	CSS	ABL	CBL	VS	BVS
Sn^{VI}	46.5	$Sn_{0.90}Al_{0.10}$	46.3	2.057	2.075	3.90	3.75
Zn^{IV}	21.8	$Zn_{0.49}Al_{0.34}Mn_{0.10}Sn_{0.07}$	21.6	1.940	1.911	2.48	2.15
$Al1^{IV}$	17.5	$Al_{0.62}Fe^{3+}_{0.38}$	17.9	1.841	1.808	3.00	2.68
$Al2^{VI}$	13.0	$Al_{1.00}$	13.0	1.889	1.935	3.00	3.15
$Al3^{VI}$	13.0	$Al_{1.00}$	13.0	1.918	1.935	3.00	2.93
$Al4^{VI}$	9.4	$Al_{0.72}$	9.4	1.956	1.785	3.00	2.64

TABLE 2b. Assigned site-occupancies in the crystal structure of zinconigerite-6*N*6*S*

Site	RSS	Site population (apfu)	CSS	ABL	CBL	VS	BVS
Sn^{VI}	48.5	$Sn_{0.92}Ti_{0.08}$	47.8	2.057	2.083	4.00	3.93
$Zn1^{IV}$	21.8	$Zn_{0.50}Fe^{3+}_{0.23}Mn_{0.14}Mg_{0.08}Al_{0.05}$	26.1	1.957	1.950	2.28	2.14
$Zn2^{IV}$	21.8	$Zn_{0.37}Al_{0.21}Fe^{3+}_{0.20}Mn_{0.14}Mg_{0.08}$	23.5	1.924	1.920	2.41	2.27
$Al1^{IV}$	17.5	$Al_{0.67}Fe^{3+}_{0.33}$	17.3	1.844	1.803	3.00	2.61
$Al2^{VI}$	13.0	$Al_{1.00}$	13.0	1.915	1.935	3.00	2.94
$Al3^{VI}$	14.2	$Al_{1.00}$	13.0	1.910	1.935	3.00	2.98
$Al4^{VI}$	13.0	$Al_{1.00}$	13.0	1.921	1.935	3.00	2.91
$Al5^{VI}$	9.3	$Al_{0.72}$	9.4	1.959	1.785	3.00	2.62

Notes: RSS = Refined site scattering factor (e^-); CSS = Calculated site scattering factor (e^-); ABL = average observed bond lengths (Å); CBL = calculated bond-lengths (Å); VS = theoretical bond-valence sums (v.u.); BVS = calculated bond-valence sums (v.u.). Ideal bond-distances are calculated using the ionic radii of Shannon (1976) and the bond-valence parameters are taken from Brown and Altermatt (1985).

TABLE 3a. Selected bond distances (Å) in zinconigerite-2*N*1*S*

Sn-O4(×3)	1.998(2)	Zn-O1	1.973(5)	Al1-O3	1.853(5)
Sn-O5(×3)	2.114(3)	Zn-O2(×3)	1.924(2)	Al1-O5(×3)	1.832(2)
<Sn-O>	2.056	<Zn-O>	1.936	<Al-O>	1.837
Al3-O1	1.924(3)	Al4-O5(×4)	1.977(3)	Al2-O2(×6)	1.899(3)
Al3-O2(×2)	1.949(2)	Al4-O6(×2)	1.914(2)	<Al-O>	1.899
Al3-O3	1.951(3)	<Al-O>	1.956		
Al3-O4(×2)	1.873(2)				
<Al-O>	1.920				

TABLE 3b. Selected bond distances (Å) in zinconigerite-6*N*6*S*

Sn-O3(×3)	2.106(3)	Zn1-O4	1.952(4)	Zn2-O2	1.960(4)
Sn-O6(×3)	2.002(1)	Zn1-O5(×3)	1.960(1)	Zn2-O7(×3)	1.921(2)
<Sn-O>	2.054	<Zn-O>	1.958	<Zn-O>	1.931
Al1-O3(×3)	1.834(2)	Al2-O2(×2)	1.943(1)	Al3-O5(×3)	1.919(2)
Al1-O8	1.864(4)	Al2-O5(×4)	1.902(1)	Al3-O7(×3)	1.896(2)
<Al-O>	1.842	<Al-O>	1.916	<Al-O>	1.908
Al4-O4	1.905(2)	Al5-O1(×2)	1.911(2)		
Al4-O6(×2)	1.873(1)	Al5-O3(×4)	1.981(3)		
Al4-O7(×2)	1.961(2)	<Al-O>	1.958		
Al4-O8	1.948(2)				
<Al-O>	1.920				

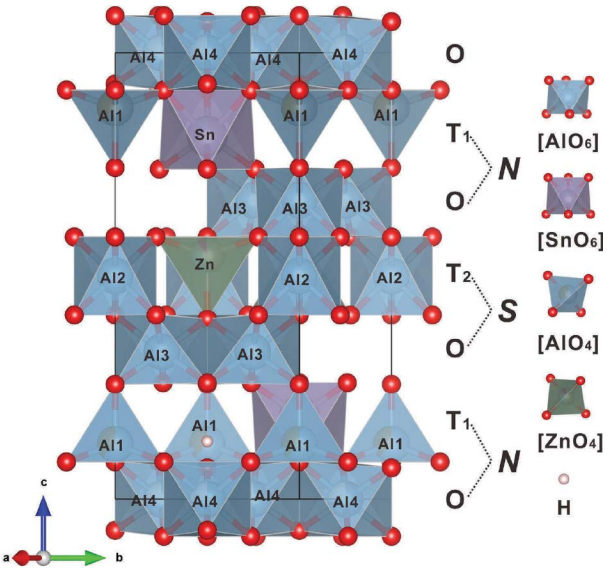

Figure 4. Crystal structure of zinconigerite-2*N*1*S*, drawn using the VESTA 3 program (Momma and Izumi 2011). (Color online.)

bond distances and bond valence sums are given in Tables 3a and 4a, respectively. The powder X-ray diffraction pattern is an excellent match to that of ferronigerite-2*N*1*S* (Arakcheeva et al. 1995), and the 10 strongest lines [*d* in Å(*I*)(*hkl*)] are 2.841(74)(104), 2.431(100)(113), 1.851(25)(211), 1.834(34)(107), 1.646(74)(214), 1.545(81)(215), 1.428(32)(220), 1.417(27)(305), 1.365(28) (223), and 1.050(39)(325), which yield unit-cell parameters of a = 5.714 (1) Å, c = 13.821 (3) Å, and V = 390.74 (1) Å^3.

The structure of zn-2*N*1*S* is based on a closed-packed oxygen framework, with *N* and *S* modules stacked along the *c*-axis (Fig. 4). The *N* module is composed of one O-layer and one T_1-layer. The O-layer is made up of the edge-sharing Al4-octahedra (<Al-O> = 1.956 Å); the T_1-layer consists of one Sn-octahedron (<Sn-O> = 2.056 Å), and one Al1-tetrahedron (<Al-O> = 1.837 Å). The Al1-tetrahedra site is occupied by 0.62 apfu Al + 0.38 apfu Fe^{3+}, and only 0.72 apfu Al in the Al4-octahedral site; the H atoms are connected to O6 atoms from the O-layer, forming an (OH) group. The *S* module has the approximate formula of gahnite $ZnAl_2O_4$, consisting of one O-layer and one T_2-layer; the O-layer is made up of the edge-sharing Al3-octahedra (<Al-O> = 1.920 Å); the T_2-layer occurs between two O-layers, is composed of one Al2-octahedra (<Al-O> = 1.899 Å) and two Zn-tetrahedra (<Zn-O> = 1.936 Å) per layer in the unit cell. The site population refinement shows that the tetrahedral site is occupied by 0.49 apfu Zn, 0.34 apfu Al, 0.10 apfu Mn, and 0.07 apfu Sn (Table 2a). As shown in Figure 1, in the T_1-layers, Sn-octahedra and Al-tetrahedra are corner-sharing, forming zigzag chains along the *a*- and *b*-axes; six-member rings occur between two adjacent zigzag chains, and the (OH) is also located in the center of six-member rings. In the T_2-layers, each Al-octahedron shares corners with six Zn-tetrahedra, and one Zn-tetrahedron is located in the center of each six-member ring of the Al-octahedra and Zn-tetrahedra. The layer sequence in zn-2*N*1*S* can be described as O-T_1-O-T_2-O-T_1 (*N*-*S*-*N*); therefore, the framework of zn-2*N*1*S* is composed of two *N* (Sn > Ti) modules and one *S* (gahnite) module (Fig. 4).

Zinconigerite-6*N*6*S*. Single-crystal X-ray diffraction data were obtained on a zn-6*N*6*S* crystal fragment measuring 0.020 × 0.045 × 0.030 mm. The crystal structure of zn-6*N*6*S* (Fig. 5) was refined from total 17 379 reflections with 857 unique reflections, extracted from 3260 frames, in the range 4.4° < 2θ < 67.4°. The structure shows trigonal symmetry, a = 5.7241(2) Å, c = 55.5393(16) Å, V = 1575.96(12) Å^3, Z = 3, and was refined in the space group $R\bar{3}m$. In the final refinement cycles, all the atoms were refined anisotropically. R_1 [F_o >2 s(F_o)] and wR_2 values are 0.0224 and 0.0574, respectively. Selected bond distances are given in Table 3b, as well as the bond valence sums in Table 4b. The powder X-ray diffraction data indicates that the seven strongest lines [*d* in Å(*I*)(*hkl*)] are 2.846(34)(1.0.16), 2.436(100) (024), 2.424(39)(0.1.20), 1.553(62)(0.3.12), 1.430(61)(220), 0.955(27) (4.1.27), and 0.935(41)(241), which are well matched to those of nigerite-12R (PDF No. 38-0436). Unit-cell parameters refined from the powder data are a = 5.7090(8) Å, c = 55.5342(4) Å, and V = 1567.56(2) Å^3.

The structure of zn-6*N*6*S* is composed of six *N* modules and six *S* modules stacked along the *c*-axis (Fig. 5). The *N* module consists of one O-layer of edge-sharing Al5-octahedra (<Al-O> = 1.958 Å) and one T_1-layer of Sn-octahedra (<Sn-O> = 2.054 Å) and Al1-tetrahedra (<Al-O> = 1.842 Å). The H atoms in the T_1-layer are connected to O atoms in the O1 site of the O-layer, forming an (OH) group. The site population refinement shows that the Al5 octahedral site is only occupied by 0.72 apfu Al, the Sn octahedral site by 0.92 apfu Sn + 0.08 apfu Ti, and the Al1 tetrahedral site by 0.67 apfu Al + 0.33 apfu Fe^{3+}. The *S* module

Table 4a. Bond valence sums for zinconigerite-2*N*1*S*

	Sn	Zn	Al1	Al2	Al3	Al4	Σ
O1		0.489			0.478(×3→)		1.92
O2		0.559 (×3↓)		0.525 (×6↓)	0.447 (×2→) (×2↓)		1.98
O3			0.647(×3↓)		0.444(×3→)		1.98
O4	0.726(×3↓)				0.5490 (×2→) (×2↓)		1.82
O5	0.531(×3↓)		0.685(×3↓)			0.415 (×2→) (×4↓)	2.05
O6						0.491(×3→) (×2↓)	1.47
Σ	3.77	2.17	2.70	3.15	2.91	2.64	

Table 4b. Bond valence sums for zinconigerite-6*N*6*S*

	Sn1	Zn1	Zn2	Al1	Al2	Al3	Al4	Al5	Σ
O1								0.495 (×3→)(×2↓)	1.49
O2			0.516		0.454 (×3→)(×2↓)				1.88
O3	0.570(×3↓)			0.671 (×2→)(×3↓)				0.410(×4↓)	2.06
O4		0.542					0.503(×3→)		2.05
O5		0.530(×3↓)			0.507(×4↓)	0.485 (×2→)(×3↓)			2.03
O6	0.755 (×2→)(×3↓)						0.549(×2↓)		1.85
O7			0.573(×3↓)			0.516(×3↓)	0.433 (×2→)(×2↓)		1.95
O8				0.619(×3↓)			0.448(×3→)		1.96
Σ	3.97	2.13	2.24	2.63	2.94	3.00	2.91	2.63	

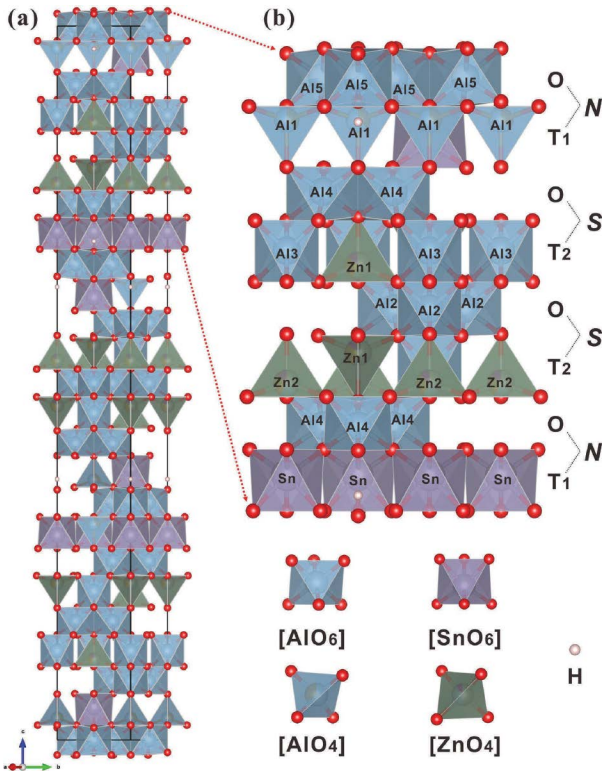

Figure 5. Crystal structure of zinconigerite-6*N*6*S* (**a**) and an enlarged view of one third of the zinconigerite-6*N*6*S* structure (**b**), showing the 2 *N* + 2*S* connectivity with the polyhedral stacking sequence of O-T_1-O-T_2-O-T_2-O-T_1. Drawn using the VESTA 3 program (Momma and Izumi 2011). (Color online.)

consists of one O-layer of edge-sharing Al2-octahedra (<Al-O> = 1.916 Å) and Al4-octahedra (<Al-O> = 1.920 Å), one T_2-layer formed by Al3-octahedra (<Al-O> = 1.908 Å) and Zn-tetrahedra (<Zn-O> = 1.944 Å). The Zn1 and Zn2 sites are occupied by 0.50 apfu Zn + 0.23 apfu Fe^{3+} + 0.14 apfu Mn + 0.08 apfu Mg + 0.05 apfu Al and 0.37 apfu Zn + 0.21 apfu Al + 0.20 apfu Fe^{3+} + 0.14 apfu Mn + 0.08 apfu Mg, respectively. As shown in Figure 1, in the O-layers, edge-sharing Al-octahedra form chains running along the *a*- and *b*-axes. In the T_1-layers, Sn-octahedra and Al-tetrahedra are adjacent to each other, forming zigzag chains along the *a*- and *b*-axes, (OH) group is also located in the center of the six-member rings of the Sn-octahedra and Al-tetrahedra. The Al- octahedra and Zn-tetrahedra in the T_2-layers are adjacent to each other, forming zigzag chains along the *a*- and *b*-axes. The layer sequence in zn-6*N*6*S* can be described as 3 × (O-T_1-O-T_2-O-T_2-O-T_1) (Fig. 5b), suggestive of a *N* + *S* + *S* + *N* + *N* + *S* + *S* + *N* + *N* + *S* + *S* + *N* connectivity of polysomatic structure (Fig. 5a).

Discussion

Crystal chemistry and substitution mechanisms

Nigerite group minerals are the members of nolanite-spinel polysomatic series, and several minerals of nigerite group have been reported (e.g., Bannister et al. 1947; Jacobson and Webb 1947; Chen et al. 1989; Yang et al. 2013). The descriptions of these phases have demonstrated that the chemical composition, number, and ratio of both nolanite and spinel modules are responsible for the polysome determination among the nolanite-spinel polysomatic series. The Zn contents (0.992 apfu for zn-2*N*1*S* and 1.736 apfu for zn-6*N*6*S*, Table 1) and structural data (Table 2) indicate the occurrence of a gahnite-type module in nolanite-spinel polysomatic series. Zn-2*N*1*S* and zn-6*N*6*S* are thus the first known polysomes with gahnite modules in nigerite group minerals. The structure of zn-2*N*1*S* shows a periodic stacking sequence of O-T_1-O-T_2-O-T_1 along the *c*-axis, reflecting the connectivity of two *N* and one *S* modules, while the layer sequence of zn-6*N*6*S* is 3 × (O-T_1-O-T_2-O-T_2-O-T_1), exhibiting a connectivity of 6*N* + 6*S* polysomatic model.

Normally, nigerite group and related minerals show trigonal ($P\bar{3}m1$ and $R\bar{3}m$) and/or hexagonal ($P6_3mc$) symmetries. The structures with an odd sum of *N* and *S* modules commonly have the symmetry of $P\bar{3}m1$, while those with an even sum of both *N* and *S* modules show $P6_3mc$ symmetry (Verma and Krishna 1966). However, zn-6*N*6*S,* with even sum of *N* and *S* modules, is trigonal with the space group of $R\bar{3}m$ (Fig. 5). This may be attributed to its O-layers sandwiched between two T_1-layers, with hydroxyl on both sides (Hejny and Armbruster 2002).

In the *N* modules of both zn-2*N*1*S* and zn-6*N*6*S*, the Al occupancy of O layers between two T_1-layers is <1. The Al4 site is only occupied by 0.72 apfu Al in zn-2*N*1*S*, and the Al5 site is also occupied by 0.72 apfu Al in zn-6*N*6*S*. The (OH) groups in both zn-2*N*1*S* and zn-6*N*6*S* (Fig. 4 and 5), connect with oxygen in the O-layers. The low-bond-valence sum of 1.47 v.u. observed at O6 is in agreement with it being an (OH) group, and so is the low-bond-valence sum of 1.49 v.u. at O1 in zn-6*N*6*S*. The Raman shifts at 3478 cm^{-1} (Fig. 3) also demonstrate the presence of (OH) in both zn-2*N*1*S* and zn-6*N*6*S*. In addition, all Fe occupies the tetrahedral sites in both zn-2*N*1*S* and zn-6*N*6*S*, and Fe^{3+} (0.49 Å) has a relatively smaller radius than Fe^{2+} (0.63 Å) (Shannon 1976), suggesting that Fe occurs as Fe^{3+} (Tables 1 and 2).

In the structure of zn-2*N*1*S*, the tetrahedral sites of T_2-layers are predominantly occupied by 0.49 apfu Zn but also contain 0.34 apfu Al, 0.10 apfu Mn, and 0.07 apfu Sn, and the octahedral sites in T_1-layer are occupied by 0.90 apfu Sn + 0.10 apfu Al (Table 2a). These features reflect the substitution of Al → Sn in Sn-octahedra, and (Al,Mn,Sn) → Zn in the tetrahedral sites of T_2-layers, suggesting the substitution mechanism of 2Al → Zn + Sn in the structure of zn-2*N*1*S*. The substitution of Al or Sn → Zn may agree with the low occupancy of the Al4 site. The tetrahedral sites of T_1-layers are occupied by 0.62 Al + 0.38 Fe^{3+}, reflecting the substitution of Fe^{3+} → Al in Al-tetrahedra.

Similarly, in the structure of zn-6*N*6*S* (Fig. 5; Table 2b), the octahedral sites in T_1-layers are occupied by 0.92 apfu Sn + 0.08 apfu Ti, suggesting the substitution of Ti → Sn. The Zn1 and Zn2 tetrahedral sites in T_2-layers, are occupied by 0.50 apfu Zn + 0.23 apfu Fe^{3+} + 0.14 apfu Mn + 0.08 apfu Mg + 0.05 apfu Al and 0.37 apfu Zn + 0.21 apfu Al + 0.20 apfu Fe^{3+} + 0.14 apfu Mn + 0.08 apfu Mg, respectively. These features suggest the complex substitution of Zn by multiple cations of Al, Fe^{3+}, Mn, Mg, which may be coupled with the low occupancy of Al5-octahedra. The tetrahedral Al1 sites from T_1-layers are occupied by 0.67 apfu Al + 0.33 apfu Fe^{3+}, also suggesting the substitution of Fe^{3+} → Al.

Lithium has been reported to be present in nigerite group minerals. For example, the zn-6*N*6*S* from the Tsomtsaub tin

mine (Namibia) contains up to 0.70 wt% Li_2O (Armbruster and Feenstra 2004), and the magnesionigerite-6*N*6*S* from the Xianghualing skarn has up to 0.74 wt% Li_2O, which substitutes Al^{3+} in the octahedral sites of O-layers between two T_1-layers, suggesting the substitution of Li + 2(Sn,Ti) → 3Al (Yang et al. 2013). Because it is impossible to analyze Li using EMPA, the occurrence of Li in the crystals investigated here could not be established. However, Li may substitute Al, and the low occupancy in the Al4 octahedral site (0.72 Al, zn-2*N*1*S*) and in the Al5 octahedral site (0.72 Al, zn-6*N*6*S*) may indicate the presence of a very little amount of Li in both zn-2*N*1*S* and zn-6*N*6*S*.

Unit-cell parameters and relations to other *N-S* polysomatic series minerals

Several polytypes of nigerite-högbomite minerals, 2*N*1*S*, 2*N*2*S*, 2*N*3*S*, 2*N*4*S*, 2*N*5*S*, 2*N*6*S*, 6*N*3*S*, 6*N*6*S*, 6*N*9*S*, and 6*N*12*S*, have been reported and predicted in nolanite-spinel polysomatic series (e.g., Hejny and Armbruster 2002; Armbruster 2002). However, Be occupying the tetrahedral site in nolanite modules results in a *N*′ slab, with composition $BeTM_4O_8$, where T and M represent tetrahedrally and octahedrally coordinated cations; this corresponds to taaffeite-group minerals (Armbruster 2002). Nigerite-, högbomite-, and taaffeite-group minerals thus form a supergroup of polysomatic series with *N* (*N*′) and *S* modules. The two new species of zinconigerite from the Xianghualing skarn are the first species in the supergroup shown to contain *S* modules with the approximate composition of gahnite. As such, the discovery of these phases extends the range of known chemical compositions in the *N-S* polysomatic series.

In terms of crystal structures, nigerite-högbomite-taaffeite supergroup minerals show trigonal or hexagonal symmetry, with similar values of *a* (approximately 5.72 Å), both *N* (*N*′) and *S* modules are 4.6 Å thick, and the values of *c* are multiples of 4.6 Å (*c* = n × 4.6 Å), where *n* is the total number of *N* (*N*′) and *S* modules (McKie 1963; Armbruster 2002). For subgroup-2*N*1*S*, n = 3, so *c* = 3 × 4.6 Å = 13.8 Å, and 55.2 (12 × 4.6) Å for subgroup-6*N*6*S*. Zn-2*N*1*S* and zn-6*N*6*S* from the Xianghualing skarn have *c* values of 13.84 and 55.54 Å, respectively. Due to the larger ionic radius of Zn than Fe^{3+} and Mg, zn-2*N*1*S* has a slightly larger *c* parameter than those of ferronigerite-2*N*1*S* (13.69 Å, Jacobson and Webb 1947) and magnesionigerite-2*N*1*S* (13.78 Å, Chen et al. 1989), and zn-6*N*6*S* has a slightly larger *c* parameter than that of magnesionigerite-6*N*6*S* (e.g., 55.45 Å, Yang et al. 2013); while ferronigerite-6*N*6*S* also contains about 8 wt% ZnO, zn-6*N*6*S* has a smaller *c* parameter (55.54 Å) than that of ferronigerite-6*N*6*S* (55.60 Å, Grey and Gatehouse 1979).

Chemically, zn-2*N*1*S* and zn-6*N*6*S* are similar to the 2*N*1*S*- and 6*N*6*S*-subgroups of ferronigerite, respectively, but the latter have higher Fe_2O_3 and lower ZnO contents than the former. The chemical composition of zn-6*N*6*S* is also close to that of zn-2*N*1*S*, but it has low contents of SnO_2 (20.54 vs. 28.15 wt% on average). It is easy to distinguish these two phases from other minerals of nigerite group by the contents of SnO_2 and ZnO.

Implications

We describe two new minerals, zn-2*N*1*S* and zn-6*N*6*S*, from the Xianghualing skarn (Hunan Province, China), and provide new insights into the crystal chemistry of the *N-S* polysomatic series. Zn-2*N*1*S* and zn-6*N*6*S* are two new minerals of the *N-S* polysomatic series and are the first minerals of the series to contain the gahnite module. It may be speculated that zinconigerite subgroups with gahnite and different ratios of *N-S* modules, such as 2*N*2*S*, 2*N*3*S*, 2*N*4*S*, 6*N*9*S*, 6*N*12*S*, and so on, will be found in nature.

Here, both zn-2*N*1*S* and zn-6*N*6*S* are of hydrothermal origin, crystallizing during the late stages of hydrothermal metasomatism in the Xianghualing skarn; the intimate intergrowths with fluorite (Fig. 2) reflect crystallization under F-rich conditions. The polysomatic minerals with *N* (*N*′) and *S* modules, such as ferronigerite-2*N*1*S*, ferronigerite-6*N*6*S*, magnesionigerite-6*N*6*S*, and taaffeite group minerals (Yang et al. 2013), also occur in close association with fluorite in the Xianghualing skarn. These features may suggest that high fluorine activity could promote the formation of minerals with *N* (*N*′) and *S* modules in hydrothermal fluids. However, neither of these two new phases contain F in abundances detectable by EMPA (Table 1), indicating the possible structural incompatibility of F relative to OH. Additionally, F-rich minerals in the polysomatic series of nigerite-högbomite with *N* (*N*′) and *S* modules are not found in nature. The high-Fe concentration of zn-2*N*1*S* and zn-6*N*6*S* (Table 1) may suggest the continuous Fe-Zn solid solutions of ferronigerite-2*N*1*S*–zn-2*N*1*S* and ferronigerite-6*N*6*S*–zn-6*N*6*S*. Moreover, some spinel group crystals from the Xianghualing skarn have up to 13.05 wt% SnO_2 and 12.78 wt% ZnO (Yu et al. 2018). The minerals of nigerite-högbomite polysomatic series likely originate from spinel through the exchange of (Fe + Zn) with Sn or Ti (Zakrzewski 1977). In addition, zn-2*N*1*S* and zn-6*N*6*S*, with same *N* and *S* modules but different numbers or ratios of *N* and *S* modules, are closely associated with each other in the Xianghualing skarn, likely indicating that the ordering of *N* and *S* modules during crystal growth leads to the formation of either zn-2*N*1*S* or zn-6*N*6*S*.

Acknowledgments and Funding

We thank Sergey Aksenov, one anonymous reviewer, and the technical editor for their comments and suggestions that have helped improve the quality of this paper significantly. Financial support for the research was provided by the NSF of China (Grant No. 41772031).

References cited

Arakcheeva, A.V., Pushcharovskii, D.Y., Rastsvetaeva, R.K., Kashaev, A.A., and Nadezhina, T.N. (1995) Crystal structure of nigerite-6*H*. Crystallography Reports, 40, 587–592.

Armbruster, T. (2002) Revised nomenclature of högbomite, nigerite, and taafeite minerals. European Journal of Mineralogy, 14, 389–395.

Armbruster, T., and Feenstra, A. (2004) Lithium in nigerite group minerals. European Journal of Mineralogy, 16, 247–254.

Armbruster, T., Bermanec, V., Zebec, V., and Oberhänsli, R. (1998) Titanium and iron poor zincohögbomite-16*H*, $Zn_{14}(Al,Fe^{3+},Ti,Mg)_8Al_{24}O_{62}(OH)_2$, from Nezilovo, Macedonia: Occurrence and crystal structure of a new polysome. Schweizerische Mineralogische und Petrographische Mitteilungen, 78, 469–477.

Bannister, F.A., Hey, M.H., and Stadler, H.P. (1947) Nigerite, a new tin mineral. Mineralogical Magazine and Journal of the Mineralogical Society, 28, 129–136.

Brown, I.D., and Altermatt, D. (1985) Bond-valence parameters obtained from a systematic analysis of the inorganic crystal-structure database. Acta Crystallographica, B41, 244–247.

Burke, E.A.J., Lof, P., and Hazebroek, H.P. (1977) Nigerite from the Rosendal pegmatite and aplite, Kemiö island, southwestern Finland. Bulletin of the Geological Society of Finland, 49, 151–157.

Chao, C.L. (1964) Liberite Li_2BeSiO_4, a new lithium-beryllium silicate mineral from the Nanling Ranges, South China. Acta Mineralogica Sinica, 44, 334–342 (in Chinese with English abstract). American Mineralogist, (1965), 50, 519 (abstract).

Chen, J.Z., Shi, Y.C., Pan, Z.L., and Peng, Z.Z. (1989) The crystal structure and crystal chemistry of a new mineral, penzhizongite-6H. Earth Science Journal of the Wuhan College of Geology, 14, 413–422.
Grey, I.E., and Gatehouse, B.M. (1979) The crystal structure of nigerite-24R. American Mineralogist, 64, 1255–1264.
Hejny, C., and Armbruster, T. (2002) Polysomatism in högbomite: The crystal structures of 10*T*, 12*H*, 14*T*, and 24*R* polysomes. American Mineralogist, 87, 277–292.
Higashi, T. (2001) ABSCOR. Rigaku Corporation, Tokyo.
Huang, Y.H., Du, S.H., Wang, K.H., Zhao, C.L., and Yu, Z.Z. (1958) Hsianghualite, a new beryllium mineral. Ti-chih-yueh-k'an 7, 35 (in Chinese). American Mineralogist (1960), 44, 1327–1328 (abstract).
Huang, Y.H., Du, S.H., and Zhou, X.Z. (1988) Hsianghualing rocks, deposits and minerals. Beijing Scientific Technique Press, 115–116 (in Chinese).
Jacobson, R., and Webb, J.S. (1947) The occurrence of nigerite, a new tin mineral in quartz-sillimanite-rocks from Nigeria. Mineralogical Magazine and Journal of the Mineralogical Society, 28, 118–128.
Mandarino, J.A. (1981) The Gladstone-Dale relationship. IV. The compatibility concept and its application. Canadian Mineralogist, 19, 441–450.
McKie, D. (1963) The högbomite polytypes. Mineralogical Magazine and Journal of the Mineralogical Society, 33, 563–580.
Momma, K., and Izumi, F. (2011) VESTA 3 for three dimensional visualization of crystal, volumetric and morphology data. Journal of Applied Crystallography, 44, 1272–1276.
Ockenga, E., Yalcin, Ü., Medenbach, O., and Schreyer, W. (1998) Zincohögbomite, a new mineral from eastern Aegean metabauxites. European Journal of Mineralogy, 10, 1361–1366.
Peacor, D.R. (1967) New data on nigerite. American Mineralogist, 52, 864–866.
Rao, C., Hatert, F., Dal Bo, F., Wang, R.C., Gu, X.P., and Baijot, M. (2017) Mengxianminite ($Ca_2Sn_2Mg_3Al_8[(BO_3)(BeO_4)O_6]_2$) a new borate mineral from Xianghualing skarn, Hunan Province, China, with a highly unusual chemical combination (B + Be + Sn.). American Mineralogist, 102, 2136–2141.
Rao, C., Wang, R.C., Gu, X.P., Xia, Q.K., Dong, C.W., Hatert, F., Yu, X.G., and Wang, W.M.Y. (2018) Zinconigerite-2*N*1*S*, IMA 2018-037. CNMNC Newsletter No. 44, August 2018, page 881. European Journal of Mineralogy, 30, 877–882.
Rao, C., Gu, X.P., Wang, R.C., Xia, Q.K., Cai, Y.F., Dong, C.W., Hatert, F., and Hao, Y.T. (2020a) Chukochenite, IMA 2018-132a. CNMNC Newsletter 54, February and March 2020, page 278. European Journal of Mineralogy, 32, 275–283.
Rao, C., Gu, X.P., Wang, R.C., Xia, Q.K., Hatert, F., and Dal Bo, F. (2020b) Zinconigerite-6*N*6*S*, IMA 2018-122a. CNMNC Newsletter 56, June and July 2020, page 443. European Journal of Mineralogy, 32, 443–448.
Schmetzer, K., and Berger, A. (1990) Lamellar iron-free högbomite-24*R* from Tanzania. Neues Jahrbuch für Mineralogie Monatshefte, 401–412.
Shannon, R.D. (1976) Revised crystal ionic radii and systematic study of interatomic distances in halides and chalcogenides. Acta Crystallographica, A32, 751–767.
Verma, A.R., and Krishna, P. (1966) Polymorphism and Polytypism in Crystals, p.154–162. Wiley.
Wilson, A.J.C. (1992) International Tables for X-ray Crystallography, Vol. C. Kluwer Academic Press.
Yang, Z.M., Ding, K.S., Fourestier, J.D., Mao, Q., and Li, H. (2013) Fe-rich Li-bearing magnesionigerite-6N6S from Xianghualing tin-polymetallic orefield, Hunan Province, P.R. China. Mineralogy and Petrology, 107, 163–169.
Yang, Z.M., Ding, K.S., Fourestier, J.D., Mao, Q., and Li, H. (2012) Ferrotaaffeite-2*N*′2*S*, a new mineral species, and crystal structure of Fe^{2+}-rich magnesiotaaffeite-2*N*′2*S* from the Xianghualing tin-polymetallic ore field, Hunan Province, China. Canadian Mineralogist, 50, 21–29.
Yu, X.G., Rao, C., Wang, W.M.Y., Lin, X.Q., and X, L. (2018) Mineralogical behavior and metallogenic process of Sn in the Xianghualing Skarn, Hunan Province. Geological Journal of China Universities, 24, 645–657.
Zakrzewski, M.A. (1977) Högbomite from the Fe-Ti deposit of Linganga (Tanzania). Neues Jahrb Mineral Monatsh, 8, 373–380.
Zhong, J.L. (2014) Major types and prospecting direction of nonferrous and rare polymetallic ore deposit in Xianghualing area, South China. Geology and Mineral Resource of South China, 30, 99–108.
Zhu, J.C., Wang, R.C., Lu, J.J., Zhang, H., Zhang, W.L., Xie, L., and Zhang, R.Q. (2011) Fractionation, evolution, petrogenesis and mineralization of Laiziling granite pluton, Southern Hunan Province. Geological Journal of China Universities, 17, 381–392.

Manuscript received January 21, 2021
Manuscript accepted October 26, 2021
Manuscript handled by Aaron J. Lussier

Endnote:

[1]Deposit item AM-22-107983, Online Materials. Deposit items are free to all readers and found on the MSA website, via the specific issue's Table of Contents (go to http://www.minsocam.org/MSA/AmMin/TOC/2022/Oct2022_data/Oct2022_data.html). The CIF has been peer reviewed by our Technical Editors.